Volume 1 | Number 1 | Jan 2013 | Pages 1–100

Catalysis
Science &
Technology

www.rsc.org/catalysis

ROYAL SOCIETY
OF CHEMISTRY

Journal Name

ARTICLE

Visible Light Driven Hydrogen Evolution with a Noble Metal Free CuGa₂In₃S₈ Nanoparticle System in Water

Tarek A. Kandiel,[a,b] Georgina A. M. Hutton[a] and Erwin Reisner[a,*]

$CuGa_2In_3S_8$ (CGIS) nanoparticles were synthesised by a hot-injection method and rendered water dispersible by modification with the hydrophilic ligand 3-mercaptopropionic acid (MPA). The CGIS nanoparticles were characterised by X-ray diffraction, transmission electron microscopy, X-ray photoelectron, diffuse reflectance and infrared spectroscopy as well as inductively coupled plasma optical emission spectroscopy. Photocatalytic H_2 production using the MPA modified $CuGa_2In_3S_8$ (CGIS) nanoparticles and a nickel salt under visible light irradiation was achieved from mildly acidic solution (pH 2.6) with ascorbic acid as a sacrificial electron donor. Previously, CGIS required the presence of a precious metal co-catalyst and sulfide as a sacrificial electron donor in alkaline solution to display photocatalytic activity for H_2 generation. In the reported system, visible light irradiation of the MPA modified CGIS nanoparticles with Ni salt displayed even superior sacrificial H_2 evolution activity than when employing the precious metals Pt, Rh and Ru. An external quantum efficiency of more than 12 % was achieved at λ = 540 nm, which is almost twice that previously reported for CGIS nanoparticles in the presence of a noble metal co-catalyst and sulfide as electron donor.

Introduction

Converting solar energy into molecular hydrogen (H_2) from water is an attractive approach to produce a renewable fuel.[1] Accordingly, several solar-based technologies, e.g., photovoltaic devices coupled with electrolysers,[2, 3] photoelectrochemical cells,[4-6] and photocatalytic systems,[7, 8] have been investigated to produce H_2. Photocatalytic water splitting with semiconductor powders is a particularly promising approach for sustainable H_2 production due to its simplicity, ease of scale-up and potential engineering advantages due to enhanced radial mass transfer kinetics in a stirred bulk system compared to electrode based devices.[9, 10]

The development of photocatalysts that can absorb and utilise the visible spectrum of solar light and can operate without the need for non-scalable noble metal co-catalysts is needed to make photocatalytic systems more efficient and economical.[11, 12] Commonly, metal oxide colloids have been investigated as photocatalysts for H_2 production, but their wide band gap often prevents activity without UV light.[13] Common strategies to extend the functionality of metal oxide photocatalysts toward the visible light range include doping, creation of oxygen vacancies,[14] and nitridization to prepare

oxynitrides,[15, 16] but the overall efficiencies achieved are typically low.

An alternative to metal oxides are ternary and quaternary metal sulfide photocatalysts, which have recently been identified as promising candidates for visible light driven H_2 production.[17] In contrast to binary metal sulfides such as CdS, the band gap of ternary and quaternary metal sulfides can be tuned by controlling their stoichiometry and composition.[18, 19] However, the development of a protocol for their synthesis is often challenging due to the difference in the reactivity of the cationic precursors towards binary metal sulfide formation. The ternary metal sulfide $CuGa_3S_5$ can be prepared by a solid-state method and exhibits visible light activity towards H_2 evolution from an aqueous solution containing Na_2S and Na_2SO_3 as sacrificial electron donors and particulate NiS as a co-catalyst. Nevertheless, $CuGa_3S_5$ absorbs light only up to 516 nm, which is close to that of absorption edge of CdS.[20] By inclusion of indium into $CuGa_3S_5$ using the same method, Kudo *et al.* developed a novel quaternary metal sulfide $CuGa_2In_3S_8$ (CGIS) photocatalyst, which absorbs light up to 700 nm (which therefore covers almost 50% of the solar spectrum).[21] Recently, a nano-sized CGIS photocatalyst has also been reported.[22] It showed higher activity than micro-sized particle tested under the same conditions, which might be attributed to its higher surface area and good dispersion properties.[22] The effect of the Ga to In ratio in $CuGa_xIn_{5-x}S_8$ (x = 0–5) on the photocatalytic activity was investigated and $CuGa_2In_3S_8$ showed the highest activity and stability.[23] Solar H_2 production using CGIS nanoparticles under visible light irradiation has previously only been observed in the presence of a none-scalable noble metal co-catalyst and sulfide ions as

[a.] Department of Chemistry, University of Cambridge, Cambridge, CB2 1EW, UK. E-mail: reisner@ch.cam.ac.uk; Web: http://www-reisner.ch.cam.ac.uk/
[b.] Department of Chemistry, Faculty of Science, Sohag University, Sohag 82524, Egypt.

an electron donor in alkaline solution (pH > 12).[21, 22] In this study, CGIS nanoparticles modified with hydrophilic ligands (3-mercaptopropionic acid, MPA) and tetramethylammonium hydroxide, TMAH) have been synthesised. Utilising the MPA modified CGIS nanoparticles and nickel ions, a visible light active and noble metal free system for photocatalytic H_2 production from mildly acidic solution (pH 2.6) with ascorbic acid (AA) as a sacrificial electron donor is reported.

Experimental Section

Synthesis of CuGa₂In₃S₈ nanoparticles

CuGa$_2$In$_3$S$_8$ nanoparticles were prepared by a previously reported hot-injection method with slight modification.[22] Briefly, copper(III) acetylacetonate (0.5 mmol, 98%, Acros Organics), gallium(III) acetylacetonate (1.0 mmol, 99.99% trace metals basis, Aldrich), and indium(III) acetylacetonate (1.5 mmol, 99.99% trace metals basis, Aldrich) were dissolved in 1-octadecene (20 mL, 90%, technical grade, Aldrich) and oleylamine (3 mL, 70%, technical grade, Aldrich) and stirred at room temperature for 30 min under N_2 flow. The solution was then heated to 120 °C and maintained at this temperature for 1 h to remove water. The temperature was then increased to 150 °C and 1-dodecanethiol (DDT, 8 mmol, Sigma–Aldrich) was injected rapidly into the solution under an N_2 atmosphere with continuous stirring. The temperature of the solution was maintained at 150 °C for 30 min before it was increased gradually to 270 °C over a period of 30 min. After 15 h, the mixture was cooled, and the formed nanoparticles were isolated by centrifugation and washed thoroughly with ethanol/hexane (50% v/v) and then acetone. The nanocrystals were then dried under vacuum at room temperature and denoted CGIS-DDT.

Ligand exchange with 3-mercaptopropionic acid (MPA)

The ligand exchange with MPA was carried out according to a literature procedure.[24] MPA (0. 5 mL) was added to chloroform:methanol 2:1 (15 mL) and the pH was adjusted to ca. 11 with TMAH (ca. 1.0 g in 5 mL methanol). CGIS-DDT (100 mg) was added to the MPA solution and stirred in the dark for 6 h. The CGIS-MPA nanocrystals were isolated by centrifugation and washed with ethanol and acetone, and dried under vacuum at room temperature.

Ligand exchange with tetramethylammonium hydroxide (TMAH)

The ligand exchange with TMAH was performed according to a previous report.[25] CGIS-DDT (100 mg) was dispersed in 1:1 toluene:methanol (20 mL) by sonication. To this suspension a TMAH methanolic solution (10 mL, 0.05 M) was added and the mixture was stirred in the dark for 6 h. The CGIS-TMAH nanoparticles were isolated by centrifugation and washed with ethanol and acetone and dried under vacuum at room temperature.

Characterisation

The XRD patterns of the CGIS nanoparticles were collected on a X'Pert PRO X-ray diffractometer (PANalytical B.V.). Transmission electron microscopy (TEM) was performed on a FEI Technai F20 FEG S/TEM operating at 200 kV. XPS analysis was performed using an AXIS Nova instrument (Kratos Analytical, with the CasaXPS software) using a high power monochromatic Al Kα radiation (1486.6 eV, 400 μm spot size, 36 W). Diffuse reflectance UV-vis spectroscopy (DRS) was performed on a Varian Cary 50 UV-Vis spectrophotometer equipped with a diffuse reflectance accessory. Attenuated total reflectance Fourier transform infrared (ATR-FTIR) spectroscopy was carried out on a Thermo Scientific Nicolet iS50 FT-IR spectrometer. Inductively coupled plasma optical emission spectroscopy (ICP-OES) was measured by digesting the CGIS samples in a mixture of concentrated HCl (3 mL) and concentrated HNO$_3$ (1.0 mL). After dilution to 10 mL, the ICP data were recorded using a Thermo Scientific spectrometer (iCAP 7000 series).

Photocatalytic measurements

Photocatalytic experiments were performed using a Newport Oriel solar light simulator (100 mW cm^{-2}, AM 1.5G). The light source was equipped with a water filter to remove IR irradiation and a 420 nm long-pass cut-off filter to eliminate UV irradiation. The illuminated area was approximately 13 cm^2. Samples were prepared by sonicating 3 mg CGIS nanoparticles in 3 mL of aqueous L-ascorbic acid (0.1 M, pH 2.6) for 10 min. 1.0 mL of the resulting suspension was transferred to a photoreactor (total volume 7.74 mL) followed by addition of the co-catalyst and the total solution volume was adjusted to 2 mL by adding L-ascorbic acid solution. The photoreactor was then sealed and purged with N_2 containing 2% CH$_4$ as internal GC standard for 10 min. The temperature of the photoreactor was kept at 25 °C with a temperature-controlled water bath during the experiment. The evolved H_2 gas in the headspace of the photoreactor was analysed by gas chromatography (GC, Agilent 7890A Series) at regular time intervals. The GC was equipped with a 5 Å molecular sieve column (45 °C) and a thermal conductivity detector. N_2 was used as carrier gas (flow rate: 3 mL min^{-1}). Unless otherwise stated, data presented is given as the mean of three independent experiments, with errors given as the standard error. The external quantum efficiencies (EQE) at different wavelengths were measured using Xenon lamp in LOT lamp housing equipped with a monochromator (LOT MSH300). The light intensity at the photoreactor window was adjusted to be 1 mW cm^{-2} using a Thorlabs power meter and the illuminated area was confined to be 0.28 cm^2. The EQE was calculated from the rate of H_2 evolution (r_{H_2}, mol h^{-1}), the incident photon flux (I_o, einstein h^{-1} cm^{-2}) and the illuminated area (A, cm^{-2}) according to equation (1):

$$EQE_{H_2} = \frac{r_{H_2} \times 2}{I_0 \times A} \qquad (1)$$

Results and discussion

CGIS nanoparticles were synthesised by a hot-injection method,[22] and Cu(II), Ga(III), and In(III) acetylacetonates were used as precursors for the metal cations and a 1-octadecene/oleylamine mixture was used as the solvent. DDT was used as a sulfur source and stabilising ligand and it reacts with the metal cations to form a CuInGa(SR)$_x$ thiolate complex, which decomposes on heating to form CGIS nanoparticles with the desired composition, preventing the formation of binary metal sulfides.

The composition and the crystal structure of the isolated CGIS nanoparticles were characterised by ICP-OES and XRD measurements as shown in Table 1 and Figure 1, respectively.

Table 1. Elemental composition (determined by ICP-OES) of CuGa$_2$In$_3$S$_8$ nanocrystals.

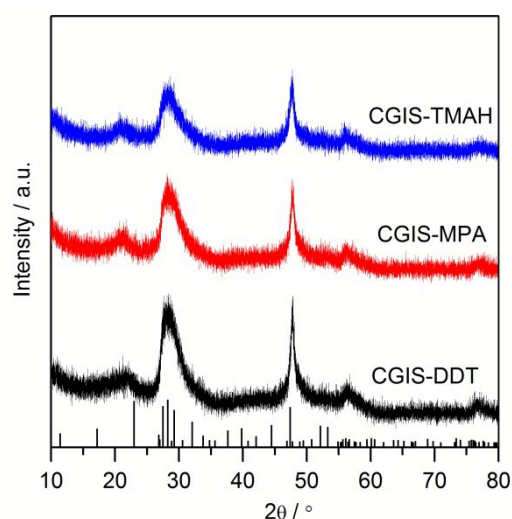| Sample ID	Atomic ratio Cu/Cu	Atomic ratio Ga/Cu	Atomic ratio In/Cu
CGIS-DDT	1	2.0	2.9
CGIS-MPA	1	2.0	2.9
CGIS-TMAH	1	2.0	3.1

Figure 1. XRD patterns of CGIS nanoparticles as prepared (CGIS-DDT), and after ligand exchange with MPA (CGIS-MPA) and TMAH (CGIS-TMAH). The vertical lines indicate Bragg positions for the layered structure of Ag$_{1.12}$Ga$_{2.68}$In$_{3.7}$S$_{10}$ (equivalent to AgGa$_2$In$_3$S$_8$, PDF 01-070-8366).

The analyses confirmed CGIS nanoparticles with the desired composition (CuGa$_2$In$_3$S$_8$) and that a layered structure similar to that of AgGa$_2$In$_3$S$_8$ is formed. Although standard XRD patterns for CuGa$_2$In$_3$S$_8$ are not available in the literature or in the JCPDS database, the CuGa$_2$In$_3$S$_8$ nanoparticles appear to have similar lattice constants to that of AgGa$_2$In$_3$S$_8$ (PDF 01-070-8366).[22, 26] The weak intensity of the diffraction peaks along the c [001] direction (that is below 2θ = 25°) might be attributable to excessively small particle sizes in this direction. The morphology of the nanoparticles was investigated by TEM,

which indicated the formation of monodisperse nanoparticles with an average diameter of 7.0±1.5 nm (Figure 2).
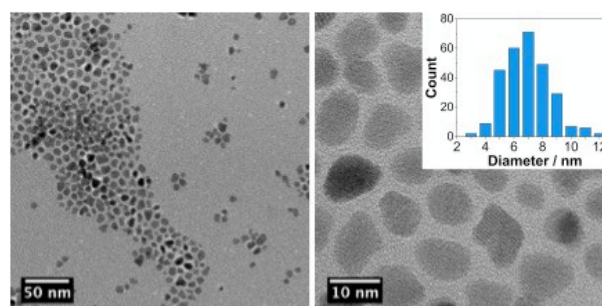

Figure 2. TEM images of CGIS nanoparticles at different magnifications. The inset shows the particle size distribution.

The as-prepared CGIS-DDT nanoparticles exhibit hydrophobic character and do not readily disperse in aqueous solution due to the surface capping with long-chain aliphatic ligands, either from oleylamine or more likely from DDT. Studying the photocatalytic activity of CGIS-DDT nanoparticles requires enhancing their dispersibility in water. Previously sulfide ions were used as an electron donor and a ligand removal agent to enhance the solubility of the particles in alkaline solution.[22, 23, 27] In this work, photocatalytic activity was investigated in acidic solution in the absence of sulfide ions and the capping ligands were exchanged with hydrophilic ligands to enhance the dispersibility of the CGIS nanoparticles. Two types of ligands were studied: MPA as a bifunctional ligand[24] and TMAH[25] as a surfactant. ATR-FTIR spectroscopy of CGIS-MPA and CGIS-TMAH nanoparticles obtained after ligand exchange indicates the effective removal of the capping ligands as the C–H stretching vibrations at ν = 2917 and 2848 cm^{-1} have almost disappeared (Figure S1). Ligand exchange was further confirmed by the dispersibility of CGIS-MPA and CGIS-TMAH in aqueous solution. Additional characterisation indicated that neither the crystal structure nor the optical properties of the CGIS nanoparticles were changed after ligand exchange as evidenced from XRD and diffuse reflectance spectroscopy (Figures 1 and 3).
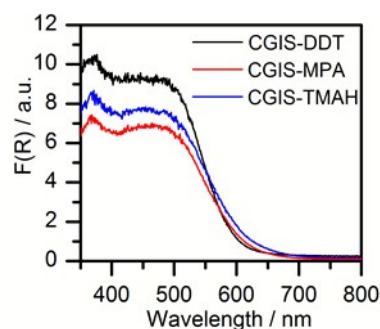

Figure 3. Diffuse reflectance UV-vis spectra of CGIS-DDT, CGIS-MPA, and CGIS-TMAH nanoparticles.

The band gap of the CGIS nanoparticles was estimated from the absorption onset as 1.85 eV, which indicates a light absorption up to 670 nm. This agrees with that reported for micro-sized CGIS particles,[21] thus a quantum confinement

effect is not observed/significant at this size. The flatband band potential of CGIS materials is known to be pH-independent up to pH 11.8 and is located at −0.56 V vs. SHE.[22] Photogenerated conduction band electrons therefore have sufficient potential to reduce protons in water and the driving force increases by approximately 60 mV with a decrease in one pH unit. Thus, the acidic pH favours the photo-generation of H_2 and the photogenerated valance band holes can readily oxidise AA. Our investigations into the pH dependency of this photocatalytic CGIS system confirmed that the highest efficiency is indeed observed under acidic conditions (pH 2.6, Figure S2). It should also be pointed out that the increase in driving force for proton reduction gained by the conduction band electron in acidic medium is at the expense of the driving force for the oxidation of the electron donor by the valance band hole assuming that its redox potential is pH-dependent.

The photocatalytic H_2 evolution activity of CGIS nanoparticles was investigated employing simulated solar light (AM 1.5G, $\lambda \geq 420$ nm) and an aqueous solution containing a sacrificial reagent (0.1 M L-ascorbic acid, pH 2.6) at 25 °C. As expected, CGIS-DDT showed negligible photoactivity in the presence and absence of a co-catalyst, due to their ineffective dispersibility in aqueous solution (Figure S3). In contrast, CGIS-MPA showed enhanced photocatalytic activity in the absence of a co-catalyst in comparison to that of CGIS-DDT, but the rate of H_2 evolution decreased over time and almost ceased after 2.5 h (Figure S3). The addition of $NiCl_2$ (optimised activity with 50 nmol, Figure S4) enhances the rate of H_2 evolution as shown in Figure 4a. Other 3d transition metal ions such as Co^{2+} and Fe^{3+} (50 nmol) were also investigated. Fe^{3+} showed a negligible effect on the rate of H_2 evolution, which implies it is not acting as a co-catalyst or is not interacting significantly with the CGIS particles. Co^{2+} reduces the photoactivity, probably due to passivation of the particle surface with Co deposits and/or mediates electron/hole recombination.[28]
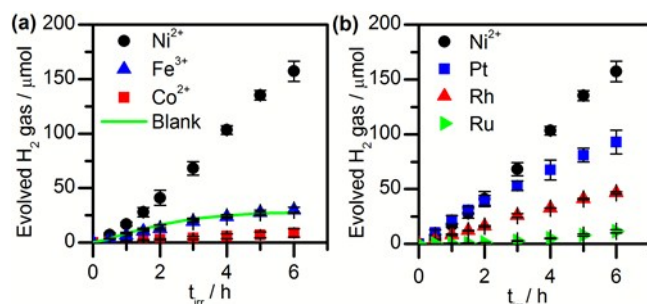

Figure 4. Visible light driven H_2 evolution with CGIS-MPA nanoparticles in the presence of (a) 3d and (b) noble metal salt co-catalysts. Conditions: 1 mg CGIS-MPA, 2 mL 0.1 M AA, pH 2.6, 1 sun illumination (AM1.5G, $\lambda > 420$ nm), 25 °C, 50 nmol metal salt (chloride salts of Ni, Co, Fe, Ru and Rh; K_2PtCl_4). The trace for CGIS-MPA + Ni^{2+} is added in part b for comparison. The blank trace in (a) was recorded without addition of a co-catalyst. Standard error is shown as a vertical bar.

CGIS nanoparticles have previously only been shown to have significantly increased activity towards photo-H_2 production in the presence of Rh and Ru noble metal co-catalysts from alkaline solution in presence of sulfide ions.[21-23]

We have also tested Pt, Rh, or Ru as co-catalysts with the CGIS-MPA nanoparticles under the current mildly acidic condition. As shown in Figure 4b, Ni^{2+} showed remarkable activity compared to that of Pt, Rh, and Ru employing the same concentration (50 nmol each, 0.29 wt.% Ni, 0.98 wt.% Pt, 0.51 wt.% Rh, and 0.5 wt.% Ru). Notably, the rate of H_2 evolution over CGIS-MPA in presence of Pt is comparable to that obtained in the presence of Ni^{2+} in the first 2 h, whereupon the Pt-modified CGIS system loses its activity over time, perhaps due to poisoning of the deposited Pt by the AA oxidation products produced at the CGIS-MPA surface.[29] The active Ni species on the other hand exhibits a homogeneous nature rather than being deposited on the CGIS-MPA surface (see below), possibly explaining its robustness under the experimental conditions employed.

The photocatalytic activity of the Ni-containing CGIS-MPA particles is independent of the nature of Ni precursor as different nickel salts (chloride, sulfate, and nitrate) displayed the same photoactivity (Figure S5). To gain further insight into the nature of the active Ni species, the CGIS-MPA photocatalyst was isolated from the reaction mixture by centrifugation after 2.5 h illumination (labelled first run in Figure 5) and the Ni concentration in the supernatant was determined by ICP-OES measurements. 90% of the Ni species remained in the solution. The isolated CGIS solid residue was re-dispersed in fresh AA (0.1 M) solution (without addition of more Ni salt) and the H_2 evolution activity is comparable to that of co-catalyst free CGIS-MPA (compare second run in Figure 5 and blank in Figure 4a). Addition of Ni^{2+} results in increased photo-H_2 evolution activity (Figure 5, third run), which confirms that the Ni species functions as a homogeneous catalyst in the presence of CGIS-MPA nanoparticles.
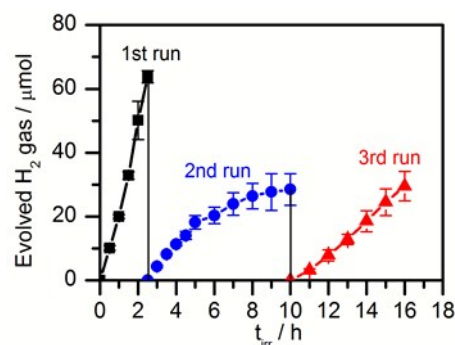

Figure 5. Visible light driven H_2 evolution with CGIS-MPA nanoparticles in the presence of 50 nmol $NiCl_2$ (1st run), after centrifugation and re-dispersion of CGIS-MPA in fresh AA solution without Ni (2nd run), and after addition of 50 nmol $NiCl_2$ (3rd run). Conditions: 1 mg CGIS-MPA, 2 mL 0.1 M AA, pH 2.6, 1 sun illumination, AM1.5G, $\lambda > 420$ nm, 25 °C.

Several Ni-thiolate compounds have previously been shown to be active for proton reduction in homogenous photocatalytic systems.[30-32] For example, a complex of Ni with dihydrolipoic acid (DHLA) was used for proton reduction with AA as an electron donor and CdSe nanocrystals capped with DHLA as light absorber.[30] A Ni complex with 2-mercaptoethanol was also used as catalyst for H_2 evolution

from homogenous system containing triethanolamine as an electron donor and Erythrosin B as a photosensitiser.[31] In heterogeneous photosystems, particulate NiS co-catalysts have also shown a considerable activity for photocatalytic H_2 evolution.[20] To investigate the possibility that Ni^{2+} ions might interact with the MPA to form Ni-MPA as an active co-catalyst for proton reduction under our conditions, the CGIS-DDT nanoparticles were modified with TMAH as hydrophilic capping ligand to render water dispersibility without the need for MPA. The CGIS-TMAH nanoparticles exhibit comparable H_2 production activity in the presence of Ni to the CGIS-MPA (Figure S3), demonstrating that the activity of the Ni species does not depend on MPA.

Photocatalytic experiments in the absence of Ni showed that the colour of the CGIS-MPA suspension gradually changes from orange-red to brown, which is accompanied by deactivation of the CGIS photocatalyst. Photogenerated holes are filled by oxidising AA and photocorrosion is not observed on this time-scale in the presence of Ni. This observation suggests photocorrosion of the CGIS nanoparticles resulting from auto-reduction of Cu(I) to Cu(0) by the photogenerated electrons.

X-ray photoelectron spectroscopy (XPS) of the CGIS-MPA nanoparticles before and after photocatalysis in the absence and presence of Ni was measured to investigate this hypothesis (Figure S6). It is evident from the Cu2p binding energies that Cu exists in the Cu^+ oxidation state due to the absence of the characteristic Cu2p3/2 satellite peak of Cu^{2+}, which should appear at approximately BE=942 eV. It was also observed that the binding energies of Cu2p, Ga2p, In3d, and S2p core in CGIS-MPA isolated after photocatalysis in the presence of Ni are identical to that of the as-prepared CGIS-MPA. In the absence of Ni, a shift towards higher binding energies (approximately 0.3 eV) was observed for all elements indicating photocorrosion of the CGIS material. Unfortunately, it was not possible to explicitly assign this shift to the reduction of Cu(I) to Cu(0) as Cu(I) and Cu(0) in sulfide compounds exhibit very close binding energies and the shift was observed for all elements.[33] It is therefore reasonable to assume that Ni ions catalyse proton reduction but the participation of Ni species in the oxidation reaction cannot be excluded. Ni was not detectable in the XPS measurements (Figure S7), further supporting that the Ni species is not deposited on the CGIS-MPA nanoparticles but rather exists in solution.

Long-term experiments showed that H_2 evolution almost ceased after approximately 9 h of full solar irradiation (λ > 300 nm), whereupon 60% of the AA has been oxidised (assuming a 2 electron oxidation, Figure 6a). Adjusting the suspension pH from 2.1 to the initial pH of 2.6 does not restore the initial rate, however, the addition of fresh AA solution significantly enhances the rate of H_2 evolution which might indicate that the main factor limiting the long-term stability of the CGIS photocatalyst is the availability of AA and the desorption of the AA oxidation product from the CGIS surface. After 9 h irradiation, 605 ± 15 µmol H_2 was produced, corresponding to a turnover number (TON_{Ni}) of

$12,100 \pm 300$ $(mol_{H2})\,(mol_{Ni})^{-1}$ confirming the catalytic nature of the Ni species. External quantum efficiency (EQE) measurements at different wavelengths were recorded for CGIS-MPA in the presence of Ni with a monochromator coupled to a Xenon lamp (Figure 6b). The EQE measurements were in excellent agreement with the diffuse reflectance spectrum of CGIS-MPA, which supports that photocatalysis proceeds through band gap excitation up to 670 nm. CGIS nanoparticles thus exhibit greater potential as visible light active photocatalysts for H_2 production than commonly investigated CdS particles, which absorb visible light only up to approximately 550 nm.[7, 34] Although it remains a challenge to maintain high EQEs at high wavelengths with CGIS, an EQE of more than 12.0% was achieved at λ = 540 nm which is almost twice that previously reported for CGIS nanoparticles in the presence of a noble metal and sulfide ions (6.5±0.5%).[22]
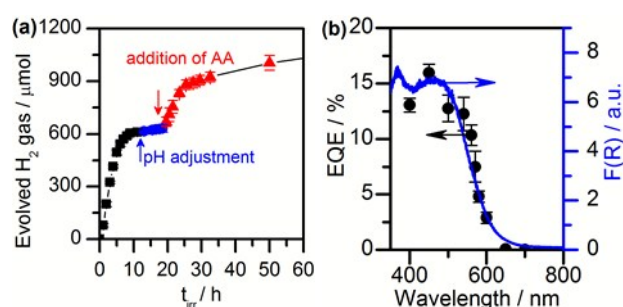

Figure 6. (a) Long-term photo-H_2 production and (b) action spectrum of CGIS-MPA nanoparticles with Ni^{2+} co-catalyst. Conditions: 1 mg CGIS-MPA, 2 mL 0.5 M AA, pH 2.6, full solar spectrum (1 sun, AM1.5G) for (a), monochromatic light (1 mW cm^{-2}) for (b), 25 °C, 50 nmol NiCl$_2$.

Conclusions

In conclusion, an efficient noble metal free system for photocatalytic H_2 evolution with CGIS nanoparticles in aqueous solution is reported. MPA-modified CGIS nanoparticles dispersed well in aqueous solution and showed high visible light driven photocatalytic activity for H_2 evolution from an aqueous solution in presence of Ni salts and AA as the electron donor. The Ni species displays better performance with CGIS-MPA than the precious metals Pt, Rh and Ru and is suggested to operate through a homogenous catalytic mechanism. Moving from alkaline to previously unexplored acidic aqueous solutions enabled the high activity of this CGIS-Ni photocatalyst system.

Acknowledgements

Notes and references

1. J. A. Turner, *Science*, 2004, **305**, 972-974.
2. B. C. M. Martindale and E. Reisner, *Adv. Energy Mater.*, 2016, **6**, 1502095.
3. J. Luo, J.-H. Im, M. T. Mayer, M. Schreier, M. K. Nazeeruddin, N.-G. Park, S. D. Tilley, H. J. Fan and M. Grätzel, *Science*, 2014, **345**, 1593-1596.
4. X. Zong, J. Han, B. Seger, H. Chen, G. Lu, C. Li and L. Wang, *Angew. Chem. Int. Ed.*, 2014, **53**, 4399-4403.
5. X. Qi, G. She, X. Huang, T. Zhang, H. Wang, L. Mu and W. Shi, *Nanoscale*, 2014, **6**, 3182-3189.
6. C.-Y. Lin, Y.-H. Lai, D. Mersch and E. Reisner, *Chem. Sci.*, 2012, **3**, 3482-3487.
7. C. M. Chang, K. L. Orchard, B. C. M. Martindale and E. Reisner, *J. Mater. Chem. A*, 2016, **4**, 2856-2862.
8. K. Maeda, K. Teramura, D. Lu, T. Takata, N. Saito, Y. Inoue and K. Domen, *Nature*, 2006, **440**, 295-295.
9. B. A. Pinaud, J. D. Benck, L. C. Seitz, A. J. Forman, Z. Chen, T. G. Deutsch, B. D. James, K. N. Baum, G. N. Baum, S. Ardo, H. Wang, E. Miller and T. F. Jaramillo, *Energy Environ. Sci.*, 2013, **6**, 1983-2002.
10. X. Gao, S. Kocha, A. J. Frank and J. A. Turner, *Int. J. Hydrogen Energy*, 1999, **24**, 319-325.
11. K. Maeda and K. Domen, *J. Phys. Chem. Lett.*, 2010, **1**, 2655-2661.
12. W. Zhang, Y. Wang, Z. Wang, Z. Zhong and R. Xu, *Chem. Commun.*, 2010, **46**, 7631-7633.
13. F. E. Osterloh, *Chem. Mater.*, 2008, **20**, 35-54.
14. T. Lin, C. Yang, Z. Wang, H. Yin, X. Lu, F. Huang, J. Lin, X. Xie and M. Jiang, *Energy Environ. Sci.*, 2014, **7**, 967-972.
15. M. Yashima, K. Maeda, K. Teramura, T. Takata and K. Domen, *Chem. Phys. Lett.*, 2005, **416**, 225-228.
16. G. Hitoki, T. Takata, J. N. Kondo, M. Hara, H. Kobayashi and K. Domen, *Chem. Commun.*, 2002, 1698-1699.
17. M. D. Regulacio and M.-Y. Han, *Acc. Chem. Res.*, 2016, **49**, 511-519.
18. C. Sun, J. S. Gardner, G. Long, C. Bajracharya, A. Thurber, A. Punnoose, R. G. Rodriguez and J. J. Pak, *Chem. Mater.*, 2010, **22**, 2699-2701.
19. K.-L. Ou, J.-C. Fan, J.-K. Chen, C.-C. Huang, L.-Y. Chen, J.-H. Ho and J.-Y. Chang, *J. Mater. Chem.*, 2012, **22**, 14667-14673.
20. M. Tabata, K. Maeda, T. Ishihara, T. Minegishi, T. Takata and K. Domen, *J. Phys. Chem. C*, 2010, **114**, 11215-11220.
21. H. Kaga, K. Saito and A. Kudo, *Chem. Commun.*, 2010, **46**, 3779-3781.
22. T. A. Kandiel, D. H. Anjum and K. Takanabe, *ChemSusChem*, 2014, **7**, 3112–3121.
23. T. A. Kandiel and K. Takanabe, *Appl. Catal. B: Environ.*, 2016, **184**, 264-269.
24. J. Aldana, N. Lavelle, Y. Wang and X. Peng, *J. Am. Chem. Soc.*, 2005, **127**, 2496-2504.
25. J. Lee, M. A. Petruska and S. Sun, *J. Phys. Chem. C*, 2014, **118**, 12017-12021.
26. H. Haeuseler, E. Elitok, A. Memo and R. Arzani, *Z. Anorg. Allg. Chem.*, 2001, **627**, 1204-1208.
27. H. Zhang, B. Hu, L. Sun, R. Hovden, F. W. Wise, D. A. Muller and R. D. Robinson, *Nano Lett.*, 2011, **11**, 5356-5361.
28. Y. Liu, J. R. Jennings, Y. Huang, Q. Wang, S. M. Zakeeruddin and M. Grätzel, *J. Phys. Chem. C*, 2011, **115**, 18847-18855.
29. K. B. Kokoh, F. Hahn, A. Métayer and C. Lamy, *Electrochim. Acta*, 2002, **47**, 3965-3969.
30. Z. Han, F. Qiu, R. Eisenberg, P. L. Holland and T. D. Krauss, *Science*, 2012, **338**, 1321-1324.
31. W. Zhang, J. Hong, J. Zheng, Z. Huang, J. Zhou and R. Xu, *J. Am. Chem. Soc.*, 2011, **133**, 20680-20683.
32. Z. Han, L. Shen, W. W. Brennessel, P. L. Holland and R. Eisenberg, *J. Am. Chem. Soc.*, 2013, **135**, 14659-14669.
33. J. F. Moudlar, W. F. Stickle, P. E. Sobol and K. D. Bomben, *Handbook of X-ray Photoelectron Spectroscopy*, Physical Electronics , Inc., USA, 1995.
34. W. Yu, T. Isimjan, S. D. Gobbo, D. H. Anjum, S. Abdel-Azeim, L. Cavallo, A. T. Garcia-Esparza, K. Domen, W. Xu and K. Takanabe, *ChemSusChem*, 2014, **7**, 2575-2583.

Table of Contents artwork
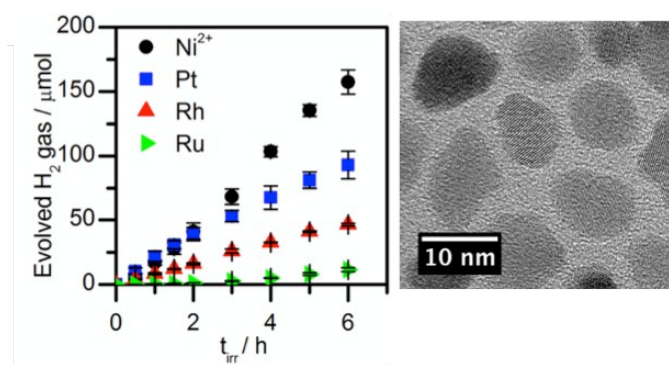
Visible light irradiation of CGIS nanoparticles with a Ni salt displayed superior sacrificial H_2 evolution activity than when employing the precious metals Pt, Rh and Ru.